NJC

PAPER

View Article Online
View Journal | View Issue

Cite this: *New J. Chem.*, 2021, **45**, 13847

Synthesis of hybrids thiazole–quinoline, thiazole–indole and their analogs: *in vitro* anti-proliferative effects on cancer cell lines, DNA binding properties and molecular modeling†

Paulo Fernando da S. Santos-Junior,‡[a] Igor José dos S. Nascimento,‡[a] Edjan Carlos D. da Silva,[a] Kadja Luana C. Monteiro,[a] Johnnatan D. de Freitas,[b] Samaysa de Lima Lins,[c] Thamilla Maria S. Maciel,[d] Bruno C. Cavalcanti,[e] José de Brito V. Neto,[e] Fabiane C. de Abreu,[c] Isis M. Figueiredo,[d] Josué Carinhanha C. Santos,[d] Claudia do Ó Pessoa,[e] Edeildo F. da Silva-Júnior,[a] João X. de Araújo-Júnior[a] and Thiago M. de Aquino *[a]

A convenient synthesis under ultrasound (US) irradiation of 4-thiazolidinone, thiazole, dihydrothiazole, and thiazine hybrid compounds containing quinoline and indole nucleus is described. All the title compounds were characterized by NMR and HRMS. The synthetic protocol affords highly selective conversions, short reaction times, simple work-up procedures, and good yields compared with conventional methods. All the synthesized compounds were tested for *in vitro* cytotoxic activity against glioblastoma (SF-295), leukemia (HL-60), and prostate cancer (PC-3) cell lines. Three compounds (**4c–e**) presented moderate to high activity against all cancer cell lines evaluated. Compound **4c** stood out with its promising cytotoxicity activity against the HL-60 cell line with an IC_{50} value of 2.41 μM and an SI of 10.5. The electrochemical behavior of **4c** was studied using differential pulse voltammetry (DPV) on a glassy carbon electrode modified with dsDNA and with ssDNA in the solution. As a result, the pre-concentration of the compound on the dsDNA biosensor surface and modification of the oxidation currents of guanosine and adenosine bases in ssDNA experiments demonstrated an interaction between **4c** and DNA. The affinity of **4c** was evaluated against ctDNA by exploring spectroscopic techniques, showing that this compound acts preferentially as a groove binder. Molecular docking and dynamics simulations proposed that **4c** interacts *via* groove binding and intercalation, corroborating the experimental results. The dominating interactions were conventional hydrogen bonds and van der Waals forces. Finally, our findings suggest the **4c** derivative to be a potential anticancer prototype against HL-60.

Received 29th April 2021,
Accepted 9th June 2021

DOI: 10.1039/d1nj02105b

rsc.li/njc

Introduction

Cancer goes back to ancient history, being found in Egyptian mummies dating back to more than 3000 years B. C.[1,2] with global economic impact measured in 2010 at approximately US$1.16 trillion.[3] Currently, it is the second leading cause of death in the world (1 in 6 deaths), with about 18.1 million cases and 9.6 million deaths reported in 2018, including lung cancer (2.09 million), breast cancer (2.09 million), and colorectal cancer (1.8 million).[4–6] Estimates have shown an increase in incidence to 29.5 million cases of cancer in 2040.[7]

In medicinal chemistry, indole and quinoline are important moieties due to their versatile activities against various diseases,[8–13] including cancer.[14–19] These heterocycles are widely found in many natural sources and have been exhaustively explored by pharmaceutical companies.[20–24] Also, thiazole is an essential 5-membered

[a] *Laboratory of Medicinal Chemistry, Institute of Pharmaceutical Sciences, Federal University of Alagoas-UFAL, Campus A. C. Simões, 57072-900, Maceió, Alagoas, Brazil. E-mail: thiago.aquino@iqb.ufal.br*
[b] *Instrumental Analysis Laboratory, Federal Institute of Alagoas-IFAL, 57020-600, Maceió, Alagoas, Brazil*
[c] *Laboratory of Electrochemistry and Microsystems for Analysis, Institute of Chemistry and Biotechnology, Federal University of Alagoas-UFAL, Campus A. C. Simões, 57072-900, Maceió, Alagoas, Brazil*
[d] *Laboratory of Instrumentation and Development in Analytical Chemistry, Institute of Chemistry and Biotechnology, Federal University of Alagoas-UFAL, Campus A. C. Simões, 57072-900, Maceió, Alagoas, Brazil*
[e] *Drug Research and Development Center-NPDM, Department of Physiology and Pharmacology, Faculty of Medicine, Federal University of Ceará-UFC, Fortaleza, Ceará, Brazil*

† Electronic supplementary information (ESI) available. See DOI: 10.1039/d1nj02105b

‡ These authors contributed equally to this work.

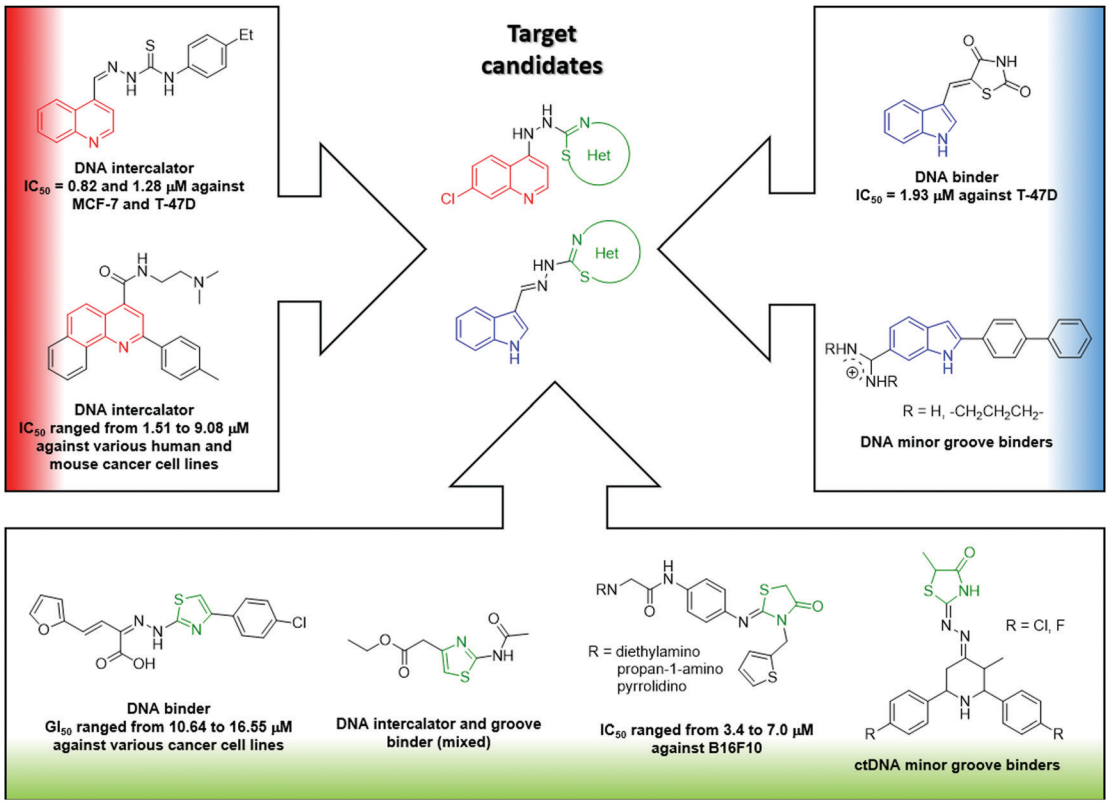

Fig. 1 Chemical structures and anticancer activities of intercalators and groove binders of DNA, and general chemical structures of designed quinoline and indole hybrid compounds.

heterocyclic compound that has increased the interest of the scientific community due to its remarkable biological activities toward several diseases[25–27] such as *Toxoplasmosis*[28,29] and *Chagas Disease*,[30,31] as well as due to its antidiabetic,[32] anti-HIV,[26,33] antimicrobial,[34] and anticancer activities.[35–41] Fig. 1 shows many anticancer compounds containing these heterocycles, especially intercalators or groove binders of DNA, which were used as starting materials for the design of the title compounds.

Some methods used for the synthesis of organic compounds feature severe reaction conditions such as high temperature and long reaction periods, which in many cases produce low yields. Given these factors, there is a need for an efficient and versatile reaction method to improve the reaction process. In this sense, the ultrasound (US) reactions are increasingly used because they are clean and environmentally sustainable, providing an alternative for preparing organic compounds of synthetic origin. Compared to conventional heating, which provides thermal energy in the macro-system, US reduces the reaction time, improves yields, and minimizes side products by providing the activation energy into the microenvironment.[42–44]

Synthetic and natural drugs exhibit high toxicity and mutation characteristics in cells, enzymes, and DNA (humans and microorganisms).[10,18] This effect on DNA can be measured using dsDNA biosensors and spectroscopic methodologies. These analyses are essential for development of new hits and lead compounds, since drug interactions with DNA are among the most critical aspects of biological and toxicological studies of pharmaceutical development processes.[3,19,20]

In this study, to explore the anticancer potential of thiazole, dihydrothiazole, 4-thiazolidinone, and thiazine analogs, we report the design and efficient conditions for US-assisted synthesis of hybrid compounds, including quinoline and indole moieties (Fig. 1). All designed compounds were screened for their ability to inhibit the *in vitro* growth of glioblastoma (SF-295), leukemia (HL-60), and prostate cancer (PC-3) cell lines. For the most active derivative (**4c**), we studied its mechanism of interaction with DNA using voltammetry, spectroscopic techniques, and *in silico* approaches.

Experimental

Chemistry

Apparatus and analysis. The chemicals and solvents were purchased from Sigma-Aldrich® and were used without further purification. ^{1}H and ^{13}C NMR spectra were recorded on a Bruker® Avance Spectrometer operating at 400 MHz and 100 MHz, respectively. The chemical shifts were reported in δ units, and coupling constants (J) were measured in hertz. The peaks are presented as s (singlet), d (doublet), t (triplet), q (quartet), quint (quintet), br s (broad singlet), dd (double doublet), td (triplet of doublets), and m (multiplet). The ultrasonic assisted reactions were carried out in a Spectralab model UMC 20 Ultrasonic

cleaner with a frequency of 40 kHz and a nominal power 250 W. Melting points were detected with open capillaries using an MSTecnopon PFMII digital melting point apparatus, and are uncorrected. All the reactions were monitored using thin layer chromatography (TLC) on aluminum-backed plates coated with Merck Kieselgel 60 F254 silica gel, and were visualized by exposure to ultraviolet light (257 nm). The purity of all compounds was determined by HPLC (Shimadzu SIL-20AHT) on a Discovery C-18 Supelco column, and methanol, methanol/formic acid, methanol/water or water was used as the mobile phase. HRMS were measured on a Bruker® microQTOF mass spectrometer.

Synthesis of 2-(7-chloroquinolin-4-yl)hydrazinecarbothioamide (2) and (E)-2-((1H-indol-3-yl)methylene)hydrazinecarbothioamide (3). See Hammoud *et al.*[45]

General procedure for the synthesis of 4a–f. To a glass tube containing a solution of **2** (1 mmol) in 5 mL of appropriate solvent (4 : 1 MeOH/DMF for **4a**, **c–f**; 4 : 1 toluene/DMF for **4b**), the required dielectrophile (1.5 eq. for **4a**, **c–f**; 4.5 eq. for **4b**) and sodium acetate (2 eq.) were added. The tube was sealed and left under ultrasonic irradiation at 85 °C until complete conversion of the starting material (20 min for **4c**; 25 min for **4d**; 35 min for **4e**, **f**; 40 min for **4b**; 55 min for **4a**). Thereafter, the reaction mixture was left to stand at room temperature, and the separated solid product was filtered off, and washed with ethyl ether and water. Finally, the final compounds were purified by recrystallization in methanol/water (**4a**, **c–f**) and column chromatography on silica gel using 9.5 : 0.5 dichloromethane/methanol (**4b**), and then dried under vacuum.

2-(2-(7-Chloroquinolin-4-yl)hydrazinyl)thiazol-4(5*H*)-one (4a). Pale yellow amorphous solid; yield: 87%; m.p. 210 °C; HPLC-UV (methanol/formic acid 0.1%): 4.72 min/99%; ^{1}H NMR (400 MHz, DMSO-d_6) δ 3.78 (2H, s, CH_2), 6.36 (1H, d, J = 7.3 Hz, ArH), 7.18 (1H, d, J = 8.2 Hz, ArH), 7.24 (2H, s, ArH), 8.09 (1H, d, J = 8.5 Hz, ArH), 10.67 (1H, br s, NH), 11.57 (1H, br s, NH); ^{13}C NMR (100 MHz, DMSO-d_6) δ 32.55, 98.40, 116.18, 119.85, 122.80, 125.58, 134.32, 134.46, 139.34, 151.54, 155.85, 173.61; HRMS (ESI$^+$) $[M + H]^+$: calcd for $C_{12}H_9ClN_4OS$: 292.0186, found: 293.0250.

2-(2-(2-(7-Chloroquinolin-4-yl)hydrazinyl)-4-oxo-4,5-dihydrothiazol-5-yl)acetic acid (4b). Yellow crystalline solid; yield: 87%; m.p. 285 °C; HPLC-UV (methanol): 2.15 min/99%; ^{1}H NMR (400 MHz, DMSO-d_6) δ 2.54 (1H, br s, NH); 2.72 (1H, s, NH from tautomer); 2.80 (1H, dd, J = 9.3 and 17.4 Hz, CH_{2a}); 2.99 (1H, dd, J = 3.7 and 17.4 Hz, CH_{2b}); 4.24 (1H, dd, J = 3.7 and 9.3 Hz, CH); 6.37 (1H, d, J = 7.6 Hz, ArH); 6.62 (1H, br s, NH); 7.17 (1H, dd, J = 2.1 and 8.6 Hz, ArH); 7.24 (2H, s, ArH); 8.01 (1H, d, J = 8.7 Hz, ArH); 10.66 (1H, br s, COOH). ^{13}C NMR (100 MHz, DMSO-d_6) δ 37.25; 43.03; 98.36; 116.21; 119.84; 122.84; 125.64; 133.92; 134.46; 139.36; 151.53; 165.91; 171.74; 174.88. HRMS (ESI$^+$) $[M + H]^+$: calcd for $C_{14}H_{10}ClN_4OS$: 318.0264. Found: 318.3044.

Ethyl 2-(2-(7-chloroquinolin-4-yl)hydrazinyl)-4-methylthiazole-5-carboxylate (4c). Pale yellow amorphous solid; yield: 90%; m.p. 282 °C; HPLC-UV (methanol/formic acid 0.1%): 1.86 min/99%; ^{1}H NMR (400 MHz, DMSO-d_6) δ 1.20 (3H, t, J = 7.0 Hz, CH_3), 2.45 (3H, s, CH_3), 4.15 (2H, q, J = 7.0 Hz, CH_2), 6.90 (1H, s, ArH), 7.80 (1H, s, ArH), 8.02 (1H, s, ArH), 8.57 (2H, m, ArH), 11.86 (1H, br s, NH); ^{13}C NMR (100 MHz, DMSO-d_6) δ 14.15; 15.94; 60.38; 98.59; 114.24; 119.06; 125.52; 127.19; 138.09; 138.64; 143.34; 161.29. HRMS (ESI$^+$) $[M + H]^+$: calcd For $C_{14}H_{10}ClN_4OS$: 318.0264, found: 318.3047.

2-(2-(7-Chloroquinolin-4-yl)hydrazinyl)-4-phenylthiazole (4d). Brown amorphous solid; yield: 92%; m.p. 295 °C; HPLC-UV (methanol/formic acid 0.1%): 2.05 min/99%; ^{1}H NMR (400 MHz, DMSO-d_6) δ 7.14 (1H, d, J = 6.8 Hz, ArH), 7.29 (1H, t, J = 7.3 Hz, ArH), 7.36–7.40 (2H, m, ArH), 7.81 (2H, m, ArH), 7.89 (1H, dd, J = 1.8 and 9.0 Hz, ArH), 8.15 (1H, d, J = 1.5 Hz, ArH), 8.65–8.67 (2H, m, ArH), 10.55 (1H, br s, NH), 11.79 (1H, br s, NH); ^{13}C NMR (100 MHz, DMSO-d_6): δ 99.08, 104.38, 113.78, 115.00, 119.41, 125.26, 125.58, 127.78, 128.61, 134.01, 138.55, 138.63, 144.01, 150.05, 15659, 169.22; HRMS (ESI$^+$) $[M - H]^+$: calcd for $C_{18}H_{11}ClN_4S$: 351.0393, found: 351.0440.

2-(2-(7-Chloroquinolin-4-yl)hydrazinyl)-4,5-dihydrothiazole (4e). Pale yellow amorphous solid; yield: 90%; m.p. 230 °C; HPLC-UV (methanol/formic acid 0.1%): 2.15 min/99%; ^{1}H NMR (400 MHz, DMSO-d_6): δ 3.64 (2H, t, J = 7.1 Hz, CH_2), 3.99 (2H, t, J = 7.4 Hz, CH_2), 6.20 (1H, d, J = 6.3 Hz, ArH), 7.40 (1H, d, J = 8.2 Hz, ArH), 7.60 (1H, s, ArH), 7.78 (1H, s, ArH), 8.30 (1H, d, J = 8.7 Hz, ArH), 8.59 (1H, s, ArH) 9.45 (1H, br s, NH); ^{13}C NMR (100 MHz, DMSO-d_6): δ 25.79, 53.15, 96.93, 117.02, 117.98, 124.05, 126.86, 136.12, 138.44, 138.63, 161.74, 165.04; HRMS (ESI$^+$) $[M + H]^+$: calcd for $C_{12}H_{11}ClN_4S$: 279.0393, found: 279.0480.

2-(2-(7-Chloroquinolin-4-yl)hydrazinyl)-5,6-dihydro-4*H*-1,3-thiazine (4f). Pale yellow amorphous solid; yield: 95%; m.p. 245 °C; HPLC-UV (methanol/formic acid 0.1%): 2.04 min/99%; ^{1}H NMR (400 MHz, DMSO-d_6); δ 2.35 (2H, s, CH_2), 3.32 (2H, s, CH_2), 3.59 (2H, s, CH_2), 6.00 (1H, d, J = 5.4 Hz, ArH), 7.39 (1H, d, J = 8.5 Hz, ArH), 7.62 (1H, s, ArH), 7.77 (1H, s, ArH), 8.04 (1H, br s, NH), 8.29 (1H, d, J = 8.8 Hz, ArH), 8.79 (1H, br s, NH from tautomer); 12.01 (1H, br s, NH); ^{13}C NMR (100 MHz, DMSO-d_6): δ 23.17, 25.79, 48.46, 96.25, 116.93, 118.21, 123.97, 127.02, 136.03, 138.60, 157.34, 161.11; HRMS (ESI$^+$) $[M + H]^+$: calcd for $C_{13}H_{13}ClN_4S$: 293.0549, found: 293.0638.

General procedure for the synthesis of 5a–f. A sealed glass tube containing a solution of **3** (1 mmol), the required dielectrophile (4.5 eq. for **5a–c**, **f**; 1.2 eq. for **5d**; 3 eq. for **5e**) and sodium acetate (3 eq. for **5a**, **d**, **f**; 2 eq. for **5c**, **e**) in 6 mL of appropriate solvent (MeOH for **5a**, **c**, **d**; toluene and drops of DMF for **5b**; isopropanol for **5e**, **f**) was left under ultrasonic irradiation at 70 °C (85 °C for **5b**) until complete conversion of the starting material (20 min for **5c**, **d**; 40 min for **5a**, **b**, **e**, **f**). After this, the reaction mixture was left to stand at room temperature, and the separated solid product was filtered off, washed with methanol and water, and dried under vacuum. Only compound **5b** was purified by recrystallization in methanol/water.

(*E*)-2-(2-((1*H*-indol-3-yl)methylene)hydrazinyl)thiazol-4(5*H*)-one (5a). White solid crystals; yield: 89%; m.p. 257–258 °C; HPLC (9 : 1 methanol/water): 3.21 min/95%; ^{1}H NMR: see Makam *et al.*;[46] ^{13}C NMR: see Makam *et al.*;[46] HRMS (ESI$^+$) $[M + H]^+$: calcd for $C_{12}H_{10}N_4OS$: 259.0575, found: 259.0634.

(*E*)-2-(2-(2-((1*H*-indol-3-yl)methylene)hydrazinyl)-4-oxo-4,5-dihydrothiazol-5-yl)acetic acid (5b). Yellow amorphous solid; yield: 80%; m.p. 230–232 °C; HPLC (methanol/formic acid 0.1%):

3.12 min/98%; ^{1}H NMR (400 MHz, DMSO-d_6): δ 2.88 (1H, dd, J = 17.3 and 8.5 Hz, CH), 3.01 (1H, dd, J = 17.5 and 3.9 Hz, CH_{2a}), 4.33 (1H, dd, J = 8.5 and 3.9 Hz, CH_{2b}), 7.13–7.21 (2H, m, ArH), 7.43 (1H, d, J = 7.3 Hz, ArH), 7.83 (1H, d, J = 2.8 Hz, ArH), 8.15 (1H, d, J = 7.0 Hz, ArH), 8.51 (1H, s, CH═N), 11.65 (1H, br s, NH), 12.26 (1H, br s, OH); ^{13}C NMR (100 MHz, DMSO-d_6): δ 36.83, 43.48, 111.96, 112.02, 120.80, 122.01, 122.77, 124.52, 131.89, 137.16, 152.52, 171.85, 175.52; HRMS (ESI$^+$) $[M + H]^+$: calcd for $C_{14}H_{12}N_4O_3S$: 317.0630, found: 317.0684.

(*E*)-ethyl 2-(2-((1*H*-indol-3-yl)methylene)hydrazinyl)-4-methylthiazole-5-carboxylate (5c). Yellow crystalline solid; yield: 94%; m.p. 255–257 °C; HPLC (water): 13.37 min/97%; ^{1}H NMR: see Makam *et al.*;[46] ^{13}C NMR: see Makam *et al.*;[46] HRMS (ESI$^+$) $[M + H]^+$: calcd for C16H16N4O2S: 329.0994, found: 329.1046.

(*E*)-2-(2-((1*H*-indol-3-yl)methylene)hydrazinyl)-4-phenylthiazole (5d). Red crystalline solid; yield: 80%; m.p. 140–142 °C; HPLC (water): 3.58 min/98%; ^{1}H NMR: see Mahmoodi *et al.*;[47] ^{13}C NMR: see Mahmoodi *et al.*;[47] HRMS (ESI$^+$) $[M + H]^+$: calcd for C18H14N4S: 319.0939, found: 319.0994.

(*E*)-2-(2-((1*H*-indol-3-yl)methylene)hydrazinyl)-4,5-dihydrothiazole (5e). Orange crystalline solid; yield: 90%; m.p. 180–182 °C; HPLC (9 : 1 methanol/water): 6.35 min/98%; ^{1}H NMR (400 MHz, DMSO-d_6): δ 3.66 (2H, t, J = 7.4 Hz, CH_2), 4.44 (2H, t, J = 7.26 Hz, CH_2), 7.18 (1H, t, J = 7.6 Hz, ArH), 7.24 (1H, t, J= 7.6 Hz, ArH), 7.49 (1H, d, J = 7.6 Hz, ArH), 8.04 (1H, d, J = 1.9 Hz, ArH), 8.38 (1H, d, J = 7.8 Hz, ArH), 8.48 (1H, s, CH═N), 10.08 (1H, br s, NH), 11.94 (1H, br s, NH); ^{13}C NMR (100 MHz, DMSO-d_6): δ 25.4, 49.68, 110.24, 112.09, 121.23, 122.50, 123.17, 123.75, 134.12, 137.15, 148.41, 166.21; HRMS (ESI$^+$) $[M + H]^+$: calcd for $C_{12}H_{12}N_4S$: 245.0783, found: 245.0888.

(*E*)-2-(2-((1*H*-indol-3-yl)methylene)hydrazinyl)-5,6-dihydro-4*H*-1,3-thiazine (5f). Yellow crystalline solid; yield: 95%; m.p. 189–190 °C; HPLC (9 : 1 methanol/water): 3.00 min/99%; ^{1}H NMR (400 MHz, DMSO-d_6): δ 2.40 (2H, quint, J = 6.0 Hz, CH_2), 3.27 (2H, t, J = 5.5 Hz, CH_2), 4.00 (2H, *t*, J = 6.0 Hz, CH_2), 7.16–7.26 (2H, m, ArH), 7.50 (1H, d, J = 7.8 Hz, ArH) 8.15 (1H, d, J = 2.9 Hz, ArH), 8.21 (1H, d, J = 7.6 Hz, ArH), 8.59 (1H, br s, NH), 8.76 (1H, s, CH═N), 9.58 (1H, br s, NH from tautomer), 12.00 (1H, br s, NH); ^{13}C NMR (100 MHz, DMSO-*d*): δ 23.28, 25.10, 46.02, 110.10, 112.17, 121.21, 121.90, 123.04, 124.11, 134.09, 137.08, 148.97, 161.23; HRMS (ESI$^+$) $[M + H]^+$: calcd for $C_{13}H_{14}N_4S$: 259.0939, found: 259.1030.

Inhibition of cell proliferation

The MTT assay was used to evaluate the cytotoxic potential of all compounds. The derivatives were diluted in DMSO and evaluated at a single concentration (10 μg mL^{-1}) in three human cancer cell lines during 72 h exposure.[48] The cell lines were SF295 (glioblastoma), HL-60 (promyelocytic leukemia), and PC3 (prostate), and were plated in 96-well microplates at a density of 0.1×10^6 (SF295 and PC3 cells) and 0.3×10^6 cells per mL (HL-60 cells). Human tumor cell lines were obtained from National Cancer Institute (Bethesda, MD, USA) and were cultured in RPMI1640 medium, supplemented with 10 or 20% fetal bovine serum and 1% antibiotics (penicillin and streptomycin). Cultures were maintained in a humidified incubator at 37 °C in a 5% CO_2 atmosphere.

An activity scale was utilized to appraise the cytotoxic potential of the tested samples: (i) inactive samples; (ii) samples with low activity (LA, cytotoxic activity between 1 and 50%); (iii) moderate activity (MA, cytotoxic activity between 50 and 75%); and (iv) high activity (HA, cytotoxic activity between 75 and 100%). Only compounds that showed moderate or high activity in at least one cell line were studied further in an expanded panel of human cell lines besides the lineages used previously: HCT-116 human colon cancer cells at a density of 0.7×10^5 cells mL^{-1}. The L929 murine fibroblast cell line (0.1×10^6 cells mL^{-1}; Rio de Janeiro Cell Bank, Brazil) was used as a model of non-cancer cells to calculate the selectivity index. After 72 h exposure to the selected compounds at a concentration ranging from 0.31 to 10 μg in prescreening, the plates were centrifuged. The medium was replaced by fresh medium (150 μL) containing 0.5 mg mL^{-1} MTT. Three hours later, the MTT formazan product was dissolved in 150 μL of DMSO, and the absorbance was measured using a multiplate reader (Spectra Count, Packard, Ontario, Canada). The drug effect was quantified as the percentage of control absorbance of the reduced dye at 595 nm. Control groups received the same amount of vehicle and doxorubicin (Doxolem®, Zodiac Produtos Farmacêuticos S/A, Brazil), the latter of which was used as a positive control. Each sample was tested in two independent experiments performed in triplicate. The results consisted of the average value for each experimental unit. The IC_{50} (cytotoxic concentration at 50% level) values and their 95% confidence intervals were obtained by nonlinear regression using the GraphPad Prism program 6 (Intuitive Software for Science, San Diego, CA).

Electrochemical studies

Cyclic voltammetry (CV) and differential pulse voltammetry (DPV) experiments were performed using a three-electrode cell, and an AutolabPGSTAT-30 potentiostat (Eco Chemie, Utrecht, Netherlands) coupled to a microcomputer, interfaced by GPES 4.9 software. A glassy carbon electrode (GC, diameter = 3 mm) was used as the working electrode, a Pt wire as the counter electrode, and an Ag/AgCl, Cl$^-$ system (saturated) as the reference electrode. The GC was cleaned by polishing with alumina on polishing felt. An inert gas was used for degassing the solution, and the solution was covered with an argon blanket during the experiments. The pH was measured (QUIMIS). All experiments were conducted at room temperature (25 °C). The solvent used in aprotic media studies was extra dry dimethylformamide (DMF) purchased from Acros Organics. Electrochemical studies in protic media were performed using a phosphate buffer pH 7.0 (ionic strength 0.2) or ethanol 5% and acetate buffer pH 4.5 (ionic strength 0.2 M).

The DNA biosensor (dsDNA) used was a Calf Thymus DNA (Sodium salt, Type I) obtained from Sigma Chemical Co, which was prepared by covering the glassy carbon electrode with 12 mg of dsDNA dissolved in 1 mL of pH 4.5 acetate buffer, which was then left in a refrigerator for 24 h for homogenization and to prevent heat degradation. Later, 10 mL was applied to the surface of the CV electrode. This DNA-modified glassy carbon electrode was then left to dry by inert gas flow and placed in the

electrochemical cell containing acetate buffer (pH 4.5). The DPV technique was used with a potential range of 0 to +1.4 V, with amplitude 0.05 V. To produce ssDNA by acid–base treatment, dsDNA (3 mg) was dissolved in 1 mL of HCl (1.0 M) by heating at 95 °C in a sealed glass tube immersed in a boiling water bath for 1 h, followed by neutralization with 1 mL of NaOH (1.0 M). A freshly prepared solution, consisting of 2 mL of ssDNA and 8 mL of acetate buffer pH 4.5, was added to the electrochemical cell. Single-scan DPV experiments were conducted between 0 and +1.4 V *versus* AgCl, KCl (0.1 M) (n = 10 mV s^{-1}, pulse amplitude = 50 mV and pulse width = 70 ms). Peaks corresponding to the oxidation of guanine and adenine appeared at +0.815 V and +1.164 V. After rinsing the surface, the GCE was immersed in a solution containing **4c** (1 to 100 mM), and the DPV experiment was repeated to observe possible interference of oxidation waves of DNA.

ctDNA spectroscopic interaction studies

Reagents and solutions. The ctDNA solution (*Calf thymus*, Sigma) was prepared by weighing 10 mg of the nucleic acid, which was solubilized in 20 mL of Tris–HCl buffer (10 mM, pH = 7.40 ± 0.10), after constant mechanical agitation for 24 h. The stock solution was stored at 4 °C. The concentration of the ctDNA solution was determined by using the absorption at 260 nm, using the molar extinction coefficient ε_{260} = 6600 L mol^{-1} at 25 °C.[49] To evaluate the purity of DNA against protein contamination, we used the ratio of absorbance at 260 and 280 nm (A_{260}/A_{280}); if the value obtained is between 1.8 and 1.9 the DNA is protein-free.[50] The stock solution (1.40 mM) of **4c** was prepared by weighing and solubilizing in dimethylsulfoxide (DMSO, Sigma), and the subsequent dilutions were prepared in Tris–HCl buffer. The maximum percentage of DMSO in the samples was 4% (v/v).[49] In the UV-vis assays, the spectra of the free **4c** (2.5 to 20 μM), **4c** bound to the ctDNA (10 μM), and the free ctDNA were measured. In the molecular fluorescence experiments, the final concentration of the fluorescent probes and the ctDNA was fixed ([EB] = [AO] = 1.5 μM, [Ho] = 0.5 μM and [ctDNA] = 6.0 μM, while [DAPI] = 1.0 μM and [ctDNA] = 10 μM) and increasing amounts of **4c** (2.5 to 120 μM, depending on the probe) were added, using a stock solution of 50 μM for all probes. In molecular fluorescence measurements, each system was excited at a specific wavelength: Ho-DNA (λ_{ex} = 350 nm), DAPI-DNA (λ_{ex} = 496 nm), EB-DNA (λ_{ex} = 525 nm) and AO-DNA (λ_{ex} = 490 nm).

Apparatus

The spectrofluorimetric titrations were carried out in an RF-5301 spectrofluorimeter (Shimadzu®, Japan) equipped with a xenon lamp (150 W) using a quartz cuvette with 10 mm optical path. UV-vis spectra were recorded in an AJX-6100PC double beam spectrophotometer (Micronal S.A., Brazil).

Docking and molecular dynamics studies

For the *in silico* study, the most stable conformation of the ctDNA (PDB entry: 1G3X) was selected after molecular dynamics (MD) simulations, as previously described by our research group.[51] Subsequently, the structure of **4c** was energetically minimized, and a blind docking was performed using Autodock Vina®.[52] The lowest energy conformation was chosen as the initial conformation for molecular dynamics (MD) simulations. MD was performed using the GROMACS® MD package. The interaction poses were visualized using UCSF Chimera and VMD® software. The RMSD values during the simulation were calculated using GROMACS®, and the RMSD chart was generated using Xmgrace® software.[52]

Results and discussion

Synthesis

In the synthesis of the title compounds, initially, thiosemicarbazide (**1**) undergoes a nucleophilic substitution with 4,7-dichloroquinoline or a condensation reaction with indole-3-carboxaldehyde, yielding thiosemicarbazone intermediates **2** and **3**, respectively, according to conventional methods described in the literature.[48] Then, 4-thiazolidinone (**4a–b** and **5a–b**), thiazole (**4c–d** and **5c–d**), dihydrothiazole (**4e** and **5e**), and thiazine (**4f** and **5f**) derivatives were prepared *via* thia-Michael cyclization, or substitution followed by intramolecular cyclization between **2** or **3** with dielectrophiles (ethyl chloroacetate, maleic anhydride, ethyl 2-chloroacetoacetate, bromo-acetophenone, dibromoethane, and dibromopropane) using US irradiation (Scheme 1).[30]

To determine the most efficient reaction conditions for the synthesis of title compounds, we compared the effects of

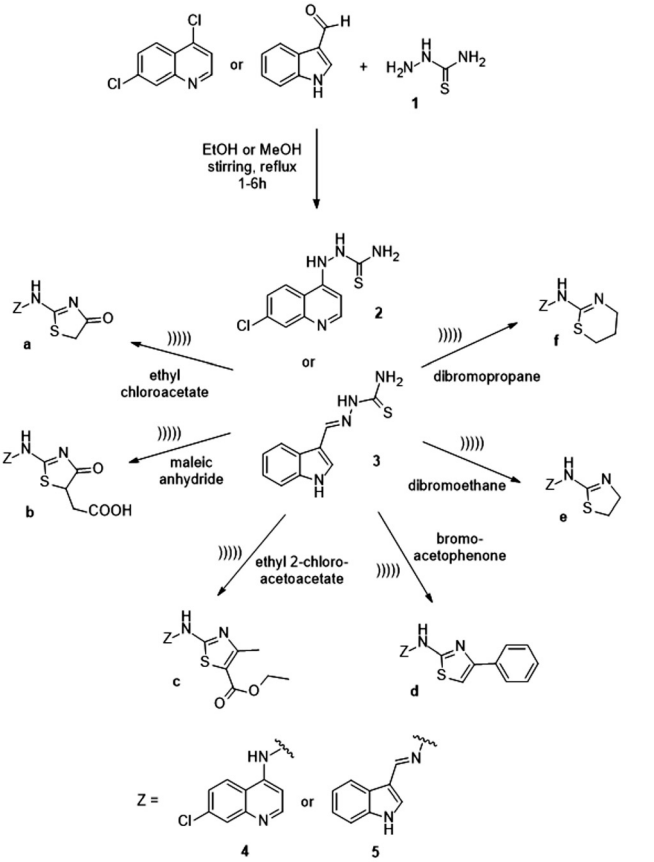

Scheme 1 Synthetic route for the thiazole, 4-thiazolidinone, dihydrothiazole and thiazine derivatives under ultrasound (US) irradiation.

Table 1 Scope of the thia-Michael cyclization or substitution followed by intramolecular cyclization involving compound **2** or **3** with dielectrophiles under ultrasound irradiation

Code	Solvent	Dielectrophile (equiv.)	T (°C)	Time (min)	Yield (%)
4a	MeOH/DMF	1.5	85	55	87
4b	Toluene/DMF	4.5	85	40	87
4c	MeOH/DMF	1.5	85	20	90
4d	MeOH/DMF	1.5	85	25	92
4e	MeOH/DMF	1.5	85	35	90
4f	MeOH/DMF	1.5	85	35	95
5a	MeOH	4.5	70	40	89
	EtOH	1.0[a]	rt[a]	120[a]	90[a]
5b	Toluene/DMF	4.5	85	40	80
5c	MeOH	4.5	70	20	94
	EtOH	1.0[a]	78[a]	60[a]	86[a]
5d	MeOH	1.2	70	20	90
	EtOH	1.0[a]	70[a]	120[a]	89[a]
5e	Isopropanol	3.0	70	40	90
5f	Isopropanol	4.5	70	40	95

[a] Conventional synthesis for **5a**, **5c**, and **5d**.[46,47,53]

ultrasound application and changing parameters such as solvent, dielectrophile equivalents, reaction time, and temperature. In this context, it was found that a mixture of toluene/DMF (ratio 4 : 1) was the appropriate solvent for the synthesis of **5b**. An increase of maleic anhydride equivalents (1.0 to 4.5 equiv.) at 85 °C accelerates the reaction time (40 min), and the desired product was isolated in 80% yield. When the small screening was extended to the synthesis of different analogs, a similar result was observed for **4b**. On the other hand, we found diverse appropriate solvents (MeOH/DMF for **4a**,**c–f**; MeOH for **5a**,**c**,**d**; isopropanol for **5e**,**f**), temperature (85 °C for **4a**, **c–f**; 70 °C for **5a**, **c–f**), and dielectrophile stoichiometry (1.5 equiv. for **4a**, **c–f**; 4.5 equiv. for **5a**,**c**,**f**; 1.2 equiv. for **5d**; 3.0 equiv. for **5e**) as the best synthetic conditions (Table 1). For all reactions performed without sodium acetate, the limiting reactants **2** and **3** were not completely consumed after 3 hours. In general, the US-assisted protocol described afforded highly selective conversions and minimum side product formation, short reaction times (20–55 min), simple work-up procedures, and high yields (80–96%). When compared with studies found in the literature, our synthesis methods increased the reaction velocity three times for indole derivatives **5a** and **5c** (Table 1).[46,47,53] The structures of the synthesized compounds were confirmed by ^{1}H NMR, ^{13}C NMR, and HRMS (see ESI†). For compounds **5a**, **5c**, **5e** **5d**, spectroscopic data were identical to that reported in the literature.[46,47,53]

Biological evaluation

The synthesized hybrid compounds **4a-f** and **5a-f** were initially screened at a single dose of 10 μg mL^{-1} (Table 2). Based on the results, in general, the compounds containing the quinoline moiety were more active than indole analogs. Derivative **4e** showed a moderate effect on the HL-60 cell line (RCV values higher than 70%), but low activity against SF295 and PC3 cells. Compound **4d** exerted a moderate cytotoxic effect on SF295 and PC3 cells but was extremely cytotoxic (greater than 90%) to HL-60. Finally, compound **4c** was very cytotoxic against all tumor lines. It exhibited cytotoxicity comparable to that of doxorubicin, especially against SF295 and PC3 cells displaying RCV values higher than 97%. Furthermore, the structure–activity relationship (SAR) for all derivatives evaluated in this study will be discussed in detail.

Table 2 Antiproliferative activity of 4-thiazolidinone, thiazole, dihydrothiazole and thiazine coupled with quinoline and indole nucleus against three different tumor cell lines

	Cell line[a]					
	SF-295		HL-60		PC-3	
Code	RVC (%)	±SD	RVC (%)	±SD	RVC (%)	±SD
2	20.7	3.8	30.9	0.8	23.5	2.7
3	27.2	4.0	2.4	2.5	9.4	3.7
4a	2.5	2.5	34.5	1.2	12.3	3.2
4b	18.2	0.5	40.8	3.0	17.2	2.9
4c	97.3	0.7	93.2	0.5	98.8	0.2
4d	79.3	0.9	91.3	0.6	79.8	1.9
4e	40.0	1.7	70.4	1.3	32.2	2.4
4f	25.8	0.9	19.4	5.9	10.1	4.6
5a	0.5	2.8	27.3	5.5	8.1	3.2
5b	19.2	2.5	35.9	5.4	3.4	2.7
5c	40.9	2.2	16.1	5.9	16.8	1.4
5d	25.6	3.1	59.8	1.5	55.9	1.3
5e	20.9	4.0	34.3	3.6	17.0	0.8
5f	17.8	1.9	34.5	2.9	16.0	5.0
DOX[b]	99.5	0.6	100	0.3	98.0	0.5

[a] All data are presented as reduction of cell viability (RCV in %) ± standard deviation (SD), obtained from two independent experiments performed in quadruplicate, after 72 hours post-incubation. [b] Doxorubicin (DOX) was employed as a positive control.

For SAR discussion of thiazole–quinoline derivatives and analogs, the quinolone-thiosemicarbazide intermediate (**2**) was initially considered the starting point by comparison with its derivatives. It was observed that this compound presents more antiproliferative effects against HL-60 cells, showing an RCV value of 30.9%. Also, it exhibits similar effects against SF-295 and PC-3 cells, with RCV values of 20.7 and 23.5%, respectively.

The cyclization of compound **2** by reaction with ethyl-2-chloroacetate provides the most poorly active derivative (**4a**). However, it presents increased activity against HL-60 cells (RCV of 34.5%) compared to its precursor. Additionally, it is possible to verify that the 4-thiazolidinone ring drastically reduces 8- and 2-fold the antiproliferative activity against SF-295 and PC-3, respectively, compared with **2**. Posteriorly, the reaction with maleic anhydride yields a derivative containing a 4-thiazolidinone substituted at position 5 by a carboxylic acid function (**4b**). It presents higher antiproliferative effects than non-substituted at 4 position (**4a**), with an RCV value of 40.8% towards HL-60 cells. Similarly to **4a**, this compound exhibits weak activity against SF-295 and PC-3 cell lines, with RCV values of 18.2 and 17.2%, respectively. The quinoline moiety, coupled to the thiazole ring substituted with methyl and ethyl ester groups at 4 and 5 positions, respectively, represents the most active derivative (**4c**) found in this study. In general, it is possible to observe that this compound exhibits a similar biological profile, showing a non-specific behavior with antiproliferative activity ranging from 93.2 to 98.8%, with a better affinity for PC-3 (RCV of 98.3%) and SF-295 (RCV of 97.3%) tumor cell lines.

The introduction of a 4-phenyl ring at the thiazole ring provides a compound (**4d**) with similar antiproliferative activity (RCV of 91.3%) against HL-60 to **4c**. In contrast, this substitution approximately reduces 20% of activity against SF-295 and PC-3 cell lines. In a sense, it can be suggested that this phenyl ring increases the affinity for HL-60 cells, generating a more selective analog. The quinoline hybrid containing a dihydrothiazole (non-substituted thiazole) ring (**4e**) presents increased activity against all three cell lines compared to its precursor **4a**. It is also verified that **4e** shows selectivity for HL-60 cells, demonstrating an RCV value of 70.4%. This compound displays low antiproliferative effects than its more substituted analogs, such as **4c** and **4d**. The replacement of the thiazole by a thiazine ring, generating compound **4f**, resulted in substantial activity reduction. This compound exhibits more affinity for SF-295 cells with a low RCV value of 25.8%.

Similarly, for SAR discussion of thiazole–indole hybrids and analogs, indole-3-thiosemicarbazide (**3**) will be used as a starting point, considering that it gives rise to the **5a–f** series of compounds. This compound presents poor activity against all cell lines evaluated, but has more affinity for SF-295 cells (RCV value of 27.2%). The introduction of a 4-thiazolidinone nucleus completely inactivates the molecule (**5a**) towards SF-295 tumor cells compared to its precursor **3**. In contrast, an increase in HL-60 antiproliferative effects is observed, showing an RCV value of 27.3%. Additionally, this compound is considered as the most inactive in this series of indole derivatives.

The insertion of a carboxylic acid function at 5 position in the thiazolidinone ring of **5a** generates a new analog (**5b**), which was inactive against HL-60 and showed modest activity against SF-295 cells (RCV of 19.2%), in comparison with its precursor **5a**. The indole moiety coupled to the thiazole ring substituted with methyl and ethyl ester groups at 4 and 5 positions (**5c**) presents more affinity for SF-295 cells, with an RCV value of 40.9%. Also, it presents increased activity against PC-3 cells (RCV of 16.8%) and decreased activity against HL-60 cells (RCV of 16.1%) compared with its precursor **5a**. In this series of indole derivatives, the derivative containing the thiazole ring substituted with a phenyl group at 4 position was found to be the most active compound (**5d**) against both HL-60 and PC-3 cell lines, with RCV of 59.8 and 55.9%, respectively. Besides, it presents low activity for SF-295 tumor cells, showing an RCV value of 25.6%. Finally, it is observed that the non-substituted hybrid compounds containing dihydrothiazole (**5e**) and thiazine rings (**5f**) present a very similar antiproliferative profile, showing RCV values of ~20, 34, and ~17% against SF-295, HL-60, and PC-3 tumor cells, respectively. Furthermore, it is verified that the sizes of these rings are not significantly essential for antiproliferative activity.

The most active compounds were chosen to estimate IC_{50} values against cancer cell lines and murine L929 fibroblasts (as a non-cancer cell model). The cell lines were treated with different concentrations of thiazole–quinoline and dihydrothiazole–quinoline hybrids **4c–e** for 72 h, and doxorubicin was used as a positive control. All compounds were tested in duplicate in two independent experiments, and the IC_{50} values are shown in Table 3. The derivative **4c** exhibited the lower IC_{50} value (2.41 μM) against HL-60 leukemic cells and the best selectivity index among the compounds tested. This compound has similar cytotoxic effects against HL-60 cells as thiazoloindolo[3,2-*c*]quinoline and thiazole derivatives, exhibiting a moderate-to-strong activity.[54,55] Finally, the analogs **4d** and **4e** exhibited low SI values (1.9 and 1.4, respectively), revealing that these compounds are not selected due to their high cytotoxicity.

Table 3 IC_{50} values for the most promising thiazole–quinoline and dihydrothiazole–quinoline hybrid compounds against different tumor and murine (L929) cell lines

	IC_{50} (μM)[a]				
Code	PC-3	HL-60	SF-295	L929	SI[c]
4c	20.7 ± 4.9	2.41 ± 0.85	>7.62	25.32 ± 9.0	10.5
4d	>28.4	14.72 ± 4.32	>28.4	>8.40	1.9
4e	>5.97	25.5 ± 10.8	>5.97	>35.97	1.4
DOX[b]	0.76 ± 0.34	0.02 ± 0.01	0.24 ± 0.07	0.66 ± 0.34	33

[a] IC_{50} ± SD values were obtained from two independent experiments in duplicate, after 72 h. [b] Doxorubicin (DOX) was employed as a positive control. [c] SI was calculated as IC_{50} L929/IC_{50} HL-60.

Spectroscopic interaction studies with ctDNA

Considering the promising antitumor potential of **4c** against the HL-60 line cell and selectivity, a ctDNA interaction study was performed to understand its possible action mechanism. Preliminary studies showed that **4c** did not exhibit intrinsic fluorescence (l_{ex} = 278 and 432 nm) at concentrations up to 120 mM. Therefore, the evaluation of the interaction process directly between ctDNA and **4c** could not be performed by molecular fluorescence studies. In this way, a competition study exploring classic fluorescent probes selective to DNA was used to evaluate the binding mode of **4c** and obtain information about ctDNA binding parameters.

Molecular fluorescence studies

Several compounds cause variation in the fluorescence intensity of the probe–DNA complex, thus providing information about the mode of binding. In this sense, probes having a well-established binding mode such as Hoechst 33258 (Ho), DAPI, ethidium bromide (EB), and acridine orange (AO) have been used to evaluate the binding mode of **4c** to ctDNA. EB and AO are widely used as fluorescent probes that bind to DNA by intercalation, and in the free form, they present low emission of fluorescence. However, a considerable increase in fluorescence intensity occurs (Fig. 2) when the probe intercalates between the DNA base pairs in the presence of a hydrophobic medium. The presence of a ligand with the same DNA binding mode in the system can lead to displacement of the intercalated EB or AO and, consequently, decrease fluorescence intensity. The competition assay principle with Ho and DAPI is similar. However, they bind to DNA *via* the minor groove and have high selectivity for DNA with AT-rich base sequences.[56]

Thus, to evaluate the preferential binding mode between **4c** and ctDNA, increasing amounts of the compound were added to the system containing Ho-ctDNA, DAPI-ctDNA, EB-ctDNA, and AO-ctDNA. As shown in Fig. 2A–E, a significant change in

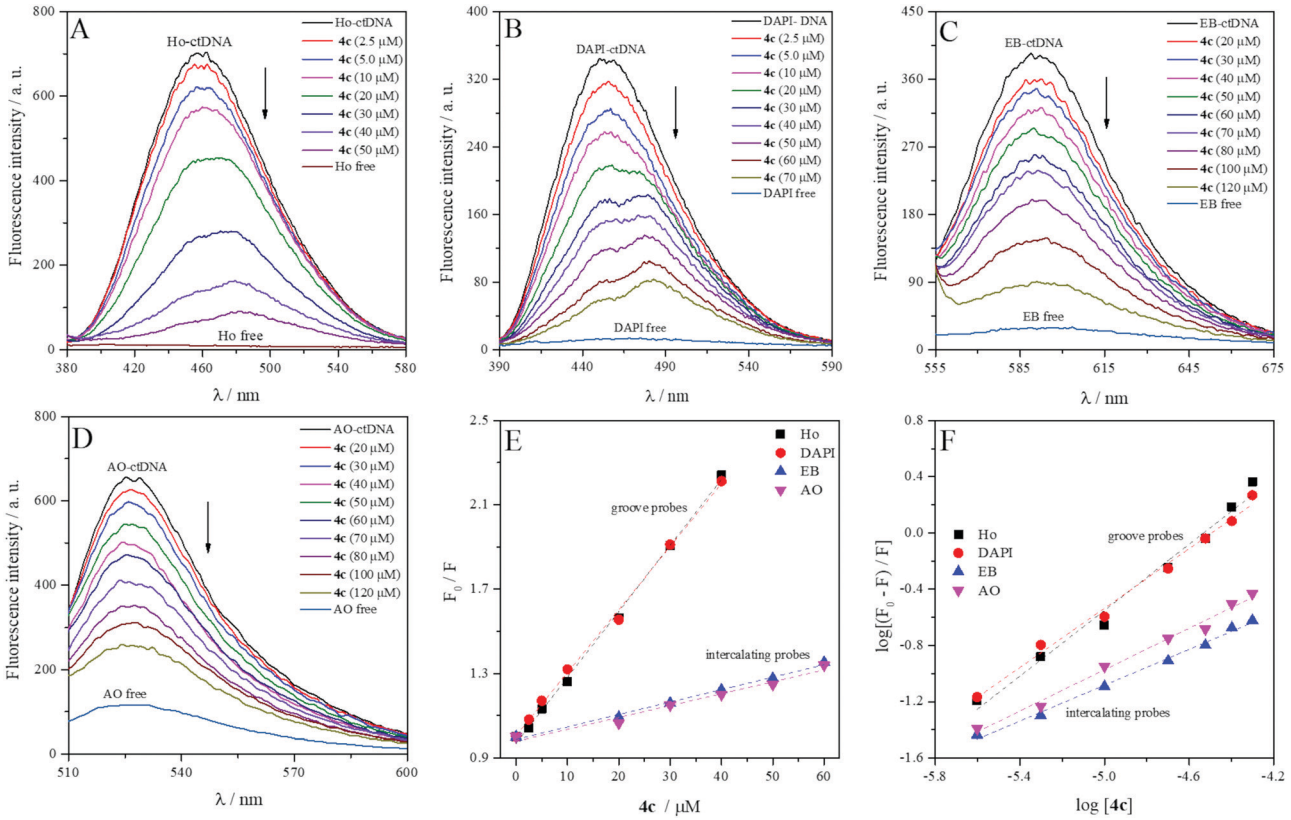

Fig. 2 Evaluation of **4c**–DNA interaction mode, (A) competition of **4c** with the Ho–ctDNA complex; (B) competition of **4c** with the DAPI–ctDNA complex; (C) competition of **4c** with the EB–ctDNA complex; (D) competition of **4c** with the AO–ctDNA complex; (E) Stern–Volmer plot for **4c** (quenching process); (F) double logarithmic curve for calculation of the binding constant of **4c** with ctDNA. Condition: pH = 7.4 (10 mM Tris–HCl) at 25 °C.

fluorescence intensity was observed with the addition of an increasing concentration of **4c**, indicating that this compound displaces the probes from the double helix and binds to the DNA *via* groove binding and intercalation.[57] This result demonstrates that the probes were displaced from DNA, suggesting that the binding mode of **4c** is groove binding and intercalation. This behavior is possibly associated with the structure of **4c**, which presents groups capable of interacting with DNA *via* both modes simultaneously.

Due to the displacement of all probes from the probe–ctDNA complex by **4c**, the information obtained by spectrofluorometric titration of this system was used to calculate the binding parameters of **4c** to ctDNA (or probe–ctDNA) and establish which mode of interaction is preferred. As previously described, when **4c** was added, there was a gradual reduction in the analytical signal. This reduction is called fluorescence quenching and is described by the Stern–Volmer equation (eqn (1)).[58,59] F_0 and F are the fluorescence intensities in the absence and presence of **4c**, respectively; [Q] is the concentration of **4c** that acts as a quencher; and K_{SV} is the quenching constant, which can be obtained by the slope of the graph F_0/F *vs.* [Q], as shown in Fig. 2E.

$$\frac{F_0}{F} = 1 + K_{SV}[Q] \quad (1)$$

Moreover, to evaluate the magnitude of the probe–ctDNA binding to **4c**, the binding constant (K_b) and the number of binding sites (n) were calculated according to eqn (2),[60] where K_b is the binding constant, n is the stoichiometric ratio, and [L] is the concentration of **4c**. The values of K_b and n are obtained from the intercept and slope, respectively, of the graph $\log[(F_0 - F)/F]$ *vs.* $\log[\mathbf{4c}]$, as shown in Fig. 2F.

$$\log\left(\frac{F_0 - F}{F}\right) = \log K_b + n \log [L] \quad (2)$$

Table 4 shows the values obtained for K_{SV} and K_b. The obtained K_{SV} value (0.56 to 3.12 × 10^4 M^{-1}) indicates the interaction between **4c** and the macromolecule (ctDNA), while the K_b value (0.023 to 4.30 × 10^5 M^{-1}) demonstrates their degree of affinity. Additionally, the value of n (0.91 to 1.18) suggests a stoichiometric ratio of 1 : 1 (**4c** : ctDNA). The results indicate that **4c** has a greater capacity to displace the Ho and DAPI probes, indicating that the preferred mode of interaction occurs *via* groove binding. However, the compounds are also intercalated with DNA.

To confirm the relative affinity and the preferred binding mode, the probabilities of intercalative DNA binding mode of **4c** were determined. The result suggests that the intercalative binding mode (%I) of **4c** constitutes 32% of the overall binding mechanism. Hence this compound is predominantly a groove binder.

The binding parameters obtained agree with works that evaluated the interaction process of similar synthetic compounds

Table 4 Values of the Stern–Volmer (K_{SV}) constants, binding constant (K_b), number of binding sites (n) and probabilities of intercalative DNA binding mode of the complex between 4c and ctDNA (or probe–ctDNA) at 25 °C

	Stern–Volmer constant		Binding parameters			Probabilities of intercalative[a] DNA by **4c**	
Probe	K_{SV} (10^4 M^{-1})	r	K_b (10^5 M^{-1})	r	n	I_{EB}/G_{DAPI}	%I
Ho	3.12 ± 0.03	0.9963	4.30 ± 0.06	0.9954	1.18 ± 0.04	0.47	32
DAPI	2.99 ± 0.04	0.9981	1.02 ± 0.10	0.9942	1.10 ± 0.05		
BE	0.59 ± 0.01	0.9955	0.023 ± 0.003	0.9796	0.91 ± 0.01		
AO	0.56 ± 0.01	0.9875	0.038 ± 0.002	0.9834	0.97 ± 0.03		

[a] Calculation criteria: $I_{50}/G_{50} = I_{EB}/I_{DAPI}$, where $I_{probe} = \log[K_{b(probe)}]/C_{50}$. The parameter C_{50} is the concentration (M) of **4c** at 50% fluorescence quenching of EB or DAPI under experimental conditions. The %I was determined as $\%I = [1 + (I_{50}/G_{50})^{-1}]^{-1} \times 100\%$.[56] K_b(DAPI) = 0.93 × 10^6 and $K_{b(EB)}$ = 7.75 × 10^6.

with DNA.[16,61–63] Additionally, Phadte *et al.*[64] and Williams *et al.*[65] have reported several bioactive compounds (dibenzodioxins, phenazines, amaranth, berenil, and imipramine, among others) that interact with DNA by intercalation and groove binding simultaneously, but with one of these modes being the preferred. Thus, the biological activity of **4c** against human tumor cells may be associated with its capacity to interact with DNA.

UV-VIS interaction studies

In this assay, the absorption spectra of the ctDNA, free **4c**, and the respective **4c**–ctDNA complex formed are analyzed (Fig. 3). Compound **4c** exhibits maximum absorption in the visible region, in which the ctDNA does not absorb. The maximum absorption values of **4c** and ctDNA are located at 432 and 260 nm (not shown), respectively. When ctDNA was added in the solution, spectral changes occurred immediately, indicating the interaction of the compounds with ctDNA and corroborating the results of molecular fluorescence.

In the UV-vis spectra, a hypochromic effect and blue shift indicate external non-covalent binding (groove), while a redshift may be an indicator of intercalation in UV-vis studies.[66] Fig. 3 shows that by adding an amount of ctDNA, a decrease in the absorbance signal is observed, characterizing the hypochromic effect, demonstrating that **4c** is bound on the outside of the helix. However, with the addition of ctDNA at concentrations 1.5 and 2 times higher than that of **4c**, there was an increase in the absorbance signal (hyperchromic effect), and a redshift, which characterizes the bathochromic effect (based on complex spectra).

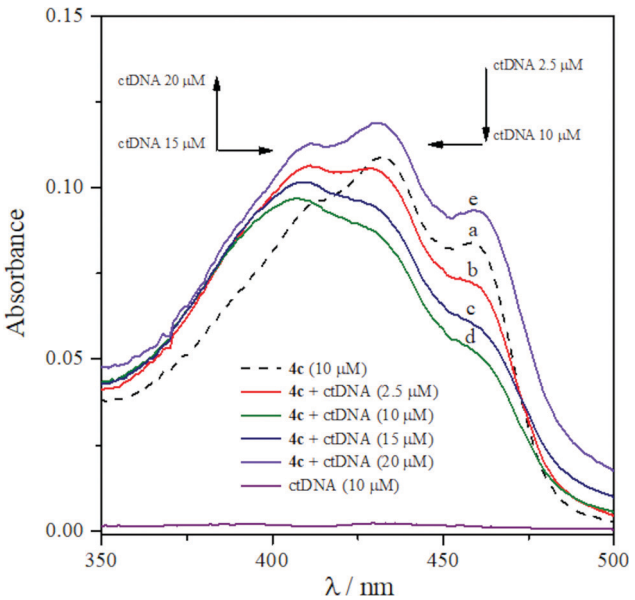

Fig. 3 Absorption spectrum of **4c** (10 μM) with increasing additions of ctDNA (0, 2.5, 10, 15 and 20 μM, curves a–e, respectively). Condition: pH = 7.4 (Tris–HCl buffer) at 25 °C.

Indeed, it is possible to infer that **4c** may change its non-covalent binding mode to the ctDNA with different biomolecule concentrations. The result suggests that **4c** interacts with ctDNA *via* the minor groove (lower concentrations of DNA) and intercalation (higher concentrations of DNA), confirming the results of molecular fluorescence. Finally, Chi *et al.*[67] and Silva *et al.*[68] have shown similar profiles by UV-vis in the studies of toluidine blue and acridine derivatives with calf thymus DNA.

Electrochemical studies

Derivative **4c** was used as a model for electrochemistry experiments and interaction with DNA. In these steps, studies using cyclic voltammetry in a protic medium were performed in a pH 7.03, 5% ethanol phosphate buffer, to promote solubility in water. Fig. 4 shows the voltammetric profile (100 μM) for this medium. The cyclic voltammogram (CV) showed a reversible system represented by E_{pc} = −0.085 V and E_{pa} = −0.056 V to 100 mV s^{-1}, which shows the oxidation of the hydrazine group (R–NH–NH–R), involving two electrons/two protons generating the Azo (R–N = N–R) derivative. These results are compatible with the studies carried out by Patai *et al.*[69] in their mechanistic studies of the oxireduction of the azo group.

Experiments of interaction with DNA demonstrate that derivative **4c** reacts with nucleic acids *in vitro*. In cases where DNA becomes the main target *in vivo*, DNA damage may also depend on the stability of the intermediate product formed by the reduction/oxidation of the bioactive compound. The electrochemical behavior of **4c** was also studied using differential pulse voltammetry (DPV) on a glassy carbon electrode modified with dsDNA. One of the dsDNA biosensor applications is the investigation of the interactions between macromolecules and biologically active compounds. The DNA biosensor is characterized by not presenting a redox response in the studied environment, and peaks of oxidation occur when the substance interacts with dsDNA, breaking hydrogen bonds and breaking its complementary base, leaving both exposed to oxidation.

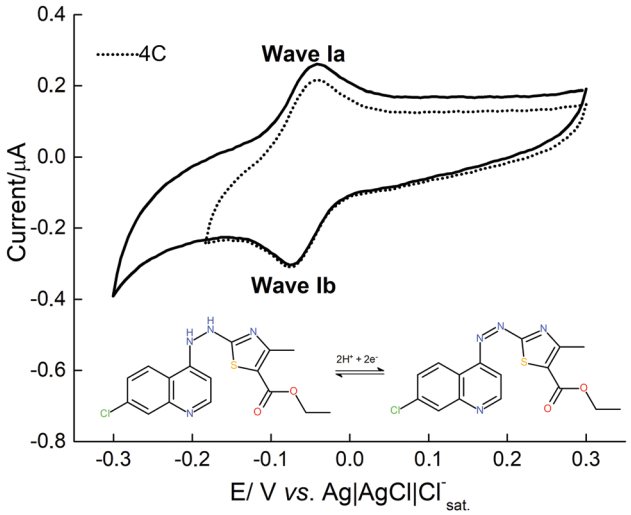

Fig. 4 Cyclic voltammogram of the electrochemical behavior of **4c** (c = 3.0 × 10^{-5} mol L^{-1}); phosphate buffer 0.2 mol L^{-1}, pH 7.03; 5% PA ethanol; CV electrode; δE: 0.3 to −0.3V.

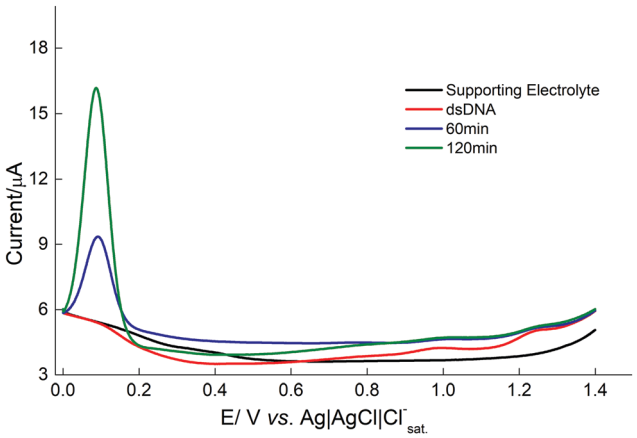

Fig. 5 Differential pulse voltammograms of dsDNA-**4c** as a function of time variation. Acetate buffer pH = 4.5; glassy carbon electrode; pulse amplitude 50 mV; pulse width 70 ms; ν = 50 mV s^{-1}.

In studies on the dsDNA biosensor, it can be seen that there are no evident changes in the voltammetric behavior in the presence of **4c**. On the other hand, its oxidation wave at E_{pa} = +0.08 V is present in the voltammogram. It is possible to observe an increase in current intensity due to the preconcentration of **4c** as a function of the contact time, proving the bioactive interaction with the double-stranded DNA (Fig. 5). When purine bases are exposed, waves of oxidation are observed around + 0.85 V, indicating the oxidation of guanine and, with a more positive potential, the oxidation of adenine.[70]

Derivative **4c** interacts with the ssDNA, a behavior that was confirmed by modifying the oxidation currents of the guanosine and adenosine bases in the ssDNA (Fig. 6A and B). In the analysis as a function of concentration, a high potential deviation from the guanine oxidation peak and disappearance of the adenine oxidation peak can be observed for high concentrations of **4c**, but at lower concentrations, the base peaks undergo potential deviation, and the peak decreases over a contact time of 60 min.

Molecular modeling

To understand the mode of interaction of **4c** with DNA, molecular docking simulation was performed. The binding pose exhibiting the lowest binding energy (−7.9 kcal mol^{-1}) was selected as the initial coordinates for the MD simulations of the DNA–ligand complex within 100 ns. The initial conformation for **4c** in the molecular dynamic simulations (from the molecular docking) is represented in Fig. 7A, where derivative **4c** binds to the DNA groove. The most prevalent conformations during MD are illustrated in Fig. 7B and C. It was observed that the compound initially remains as a groove binder, where the complex was stabilized by intermolecular van der Waals interactions (Fig. 7B). During the simulation, **4c** intercalates with DNA bases. The new pose was stabilized by conventional hydrogen bonds with residues DT20 and DA06, as well as van der Waals interactions between the quinoline moiety and the base pairs DT19 and DA06 (Fig. 7C).

The Root Mean Square Deviation (RMSD) of the DNA backbone during the simulation is presented in Fig. 7D, indicating

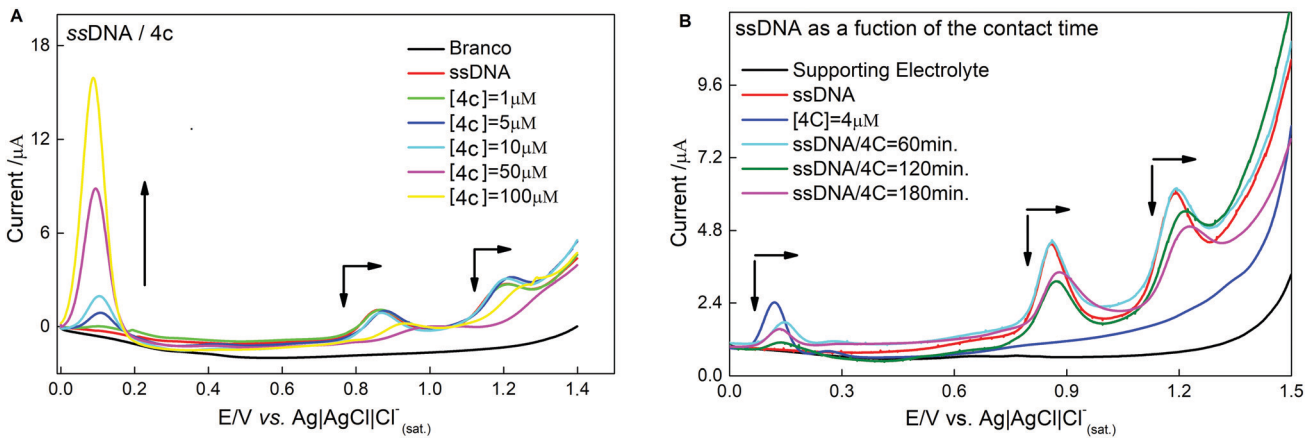

Fig. 6 (A) Differential pulse voltammograms of ssDNA in the presence of different concentrations of **4c**. Acetate buffer pH = 4.5; glassy carbon electrode; pulse amplitude 50 mV; pulse width 70 ms; ν = 50 mV s^{-1}. (B) Differential pulse voltammograms of ssDNA in the presence of **4c** as a function of time. Acetate buffer pH = 4.5. **4c**: 4.0 × 10^{-6} mol L^{-1}; glassy carbon electrode; pulse amplitude 50 mV; pulse width 70 ms; ν = 50 mV s^{-1}.

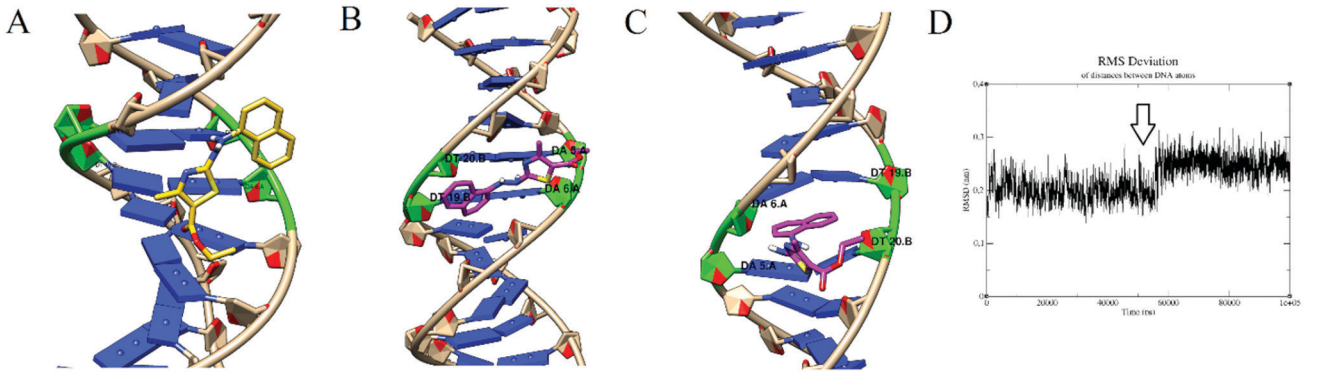

Fig. 7 (A) Best docking conformations for **4c**. (B and C) The best conformations of **4c** with DNA as a groove binder and intercalator after MD simulation, respectively. (D) RMSD plot for the DNA backbone during the molecular dynamics simulation.

that the DNA–ligand complex remains stable until the end of simulations without causing DNA denaturation. The more pronounced structural changes in the oligonucleotide occur when derivative **4c** changes from groove binding to intercalation (identified by the arrows in Fig. 7D), justified by the opening between the base pairs DT19, DT20, DA5, and DA6, as observed in Fig. 7C. Finally, Murugavel *et al.*[71] have shown a similar intercalant binding mode of some chloroquinoline derivatives with ctDNA by docking studies, due to π–π interactions involving the planar quinoline moiety and the DNA bases.

Conclusions

A series of thiazole–quinoline hybrids, thiazole–indole derivatives, and analogs have been synthesized with good yields and shorter reaction time under ultrasound irradiation. All intermediates and title compounds are characterized by NMR and HRMS. Among all derivatives screened against three cancer cell lines, some of them showed moderate to high activity, and compound **4c** displayed the lowest value of IC_{50} against HL-60 leukemic cells. The electrochemical and spectroscopic experiments established that **4c** interacts with DNA preferentially by the groove mode. The binding interactions were identified as conventional hydrogen bonds and van der Waals forces through MD simulation. Modifications to improve the potency and selectivity of this active derivative are currently in progress in our laboratory.

Author contributions

P. F. S. Santos-Junior, I. J. S. Nascimento and J. D. Freitas synthesized and provided all title compounds. S. L. Lins performed the electrochemical experiments. K. L. C. Monteiro and T. M. S. Maciel performed the spectroscopic experiments. B. C. Cavalcanti and J. B. V. Neto performed the biological assays. E. C. D. Silva performed the docking and MD studies. F. C. Abreu wrote and analyzed electrochemical results. I. M. Figueiredo and J. C. C. Santos wrote and analyzed the DNA interaction studies. C. Ó. Pessoa wrote and discussed biological results. E. F. Silva-Júnior and J. X. Araújo-Júnior wrote and revised the manuscript. T. M. Aquino designed, wrote and revised the manuscript.

Conflicts of interest

The authors declare that they have no known competing financial interests or personal relationships that could have appeared to influence the work reported in this paper.

Acknowledgements

We are grateful to the National Council for Scientific and Technological Development – CNPq (Grant numbers 308431/2017-0-CNPq-BR, 409146/2018-8-CNPq-BR, and 465536/2014-0-CNPq-BR) and Fundação de Amparo à Pesquisa do Estado de Alagoas – FAPEAL (Grant numbers: EFP_00007992-PPSUS/FAPEAL-BR) for the financial support of this work. This study was partially supported by the Coordenação de Aperfeiçoamento de Pessoal de Nível Superior – Brasil/CAPES (Finance Code 001).

Notes and references

1 E. Molto and P. Sheldrick, *Int. J. Paleopathol.*, 2018, **21**, 96–110.
2 K. J. Hunt, C. Roberts and C. Kirkpatrick, *Int. J. Paleopathol.*, 2018, **21**, 12–26.
3 P. J. McCormick, *Curr. Anesthesiol. Rep.*, 2018, **8**, 348–354.
4 R. Islam and K. W. Lam, *Eur. J. Med. Chem.*, 2020, **207**, 112812.
5 WHO, https://www.who.int/news-room/fact-sheets/detail/cancer, accessed November 30, 2020.
6 Y. Y. Tan, P. K. Yap, G. L. X. Lim, M. Mehta, Y. Chan, S. W. Ng, D. N. Kapoor, P. Negi, K. Anand, S. K. Singh, N. K. Jha, L. C. Lim, T. Madheswaran, S. Satija, G. Gupta, K. Dua and D. K. Chellappan, *Chem. – Biol. Interact.*, 2020, **329**, 109221.
7 Cancer Tomorrow, https://gco.iarc.fr/tomorrow/home, accessed November 30, 2020.
8 F. Pandolfi, F. D'Acierno, M. Bortolami, D. De Vita, F. Gallo, A. De Meo, R. Di Santo, R. Costi, G. Simonetti and L. Scipione, *Eur. J. Med. Chem.*, 2019, **165**, 93–106.
9 S. Kondaparla, A. Manhas, V. R. Dola, K. Srivastava, S. K. Puri and S. B. Katti, *Bioorg. Chem.*, 2018, **80**, 204–211.
10 H. Zhang, J. Collins, R. Nyamwihura, S. Ware, M. Kaiser and I. V. Ogungbe, *Bioorg. Med. Chem. Lett.*, 2018, **8**, 1647–1651.

11 A. Kumari and R. K. Singh, *Bioorg. Chem.*, 2019, **89**, 103021.
12 S. Pathania, R. K. Narang and R. K. Rawal, *Eur. J. Med. Chem.*, 2019, **180**, 486–508.
13 N. Chadha and O. Silakari, *Eur. J. Med. Chem.*, 2017, **134**, 159–184.
14 S. Dadashpour and S. Emami, *Eur. J. Med. Chem.*, 2018, **150**, 9–29.
15 A. M. S. El-sharief, Y. A. Ammar, A. Belal, M. A. M. S. El-sharief, Y. A. Mohamed, A. B. M. Mehany, G. A. M. E. Ali and A. Ragabet, *Bioorg. Chem.*, 2019, **85**, 399–412.
16 F. Jafari, H. Baghayi, P. Lavaee, F. Hadizadeh, F. Soltani, H. Moallemzadeh, S. Mirzaei, S. M. Aboutorabzadeh and R. Ghodsi, *Eur. J. Med. Chem.*, 2019, **164**, 292–303.
17 S. Li, L. Hu, J. Li, J. Zhu, F. Zeng, Q. Huang, L. Qiu, R. Du and R. Cao, *Eur. J. Med. Chem.*, 2019, **162**, 666–678.
18 S. Jain, V. Chandra, P. K. Jain, K. Pathak, D. Pathak and A. Vaidya, *Arabian J. Chem.*, 2019, **12**, 4920–4946.
19 A. G. Ribeiro, S. M. V. Almeida, J. F. Oliveira, T. R. C. L. Souza, K. L. Santos, A. P. B. Albuquerque, M. C. B. L. Nogueira, L. B. C. Junior, R. O. Moura, A. C. Silva, V. R. A. Pereira, M. C. A. B. Castro and M. C. A. Lima, *Eur. J. Med. Chem.*, 2019, **182**, 111592.
20 X. M. Chu, C. Wang, W. Liu, L. L. Liang, K. K. Gong, C. Y. Zhao and K. L. Sun, *Eur. J. Med. Chem.*, 2019, **161**, 101–117.
21 S. N. Chanquia, F. Larregui, V. Puente, C. Labriola, E. Lombardo and G. G. Liñares, *Bioorg. Chem.*, 2019, **83**, 526–534.
22 S. N. C. Sridhar, S. Palawat and A. T. Paul, *Bioorg. Chem.*, 2019, **85**, 373–381.
23 E. V. Nosova, G. N. Lipunova, V. N. Charushin and O. N. Chupakhin, *J. Fluorine Chem.*, 2018, **212**, 51–106.
24 T. G. Shruthi, S. Eswaran, P. Shivarudraiah, S. Narayanan and S. Subramanian, *Bioorg. Med. Chem. Lett.*, 2019, **29**, 97–102.
25 Ž. Jakopin, *Chem. – Biol. Interact.*, 2020, **330**, 109244.
26 S. K. Manjal, R. Kaur, R. Bhatia, K. Kumar, V. Singh, R. Shankar, R. Kaur and R. K. Rawal, *Bioorg. Chem.*, 2017, **75**, 406–423.
27 Y. J. Wu, *Prog. Heterocycl. Chem.*, 2020, **31**, 363–377.
28 A. P. Liesen, T. M. Aquino, C. S. Carvalho, V. T. Lima, J. M. Araújo, J. G. Lima, A. R. Faria, E. J. T. Melo, A. J. Alves, E. W. Alves, A. Q. Alves and A. J. S. Góes, *Eur. J. Med. Chem.*, 2010, **45**, 3685–3691.
29 B. Rosada, A. Bekier, J. Cytarska, W. Płaziński, O. Zavyalova, A. Sikora, K. Dzitko and K. Z. Łączkowski, *Eur. J. Med. Chem.*, 2019, **184**, 111765.
30 E. F. Silva-Júnior, E. P. S. Silva, P. H. B. França, J. P. N. Silva, E. O. Barreto, E. B. Silva, R. S. Ferreira, C. C. Gatto, D. R. M. Moreira, J. L. Siqueira-Neto, F. J. B. Mendonça-Júnior, M. C. A. Lima, J. H. Bortoluzzi, M. T. Scotti, L. Scotti, M. R. Meneghetti, T. M. Aquino and J. X. Araújo-Júnior, *Bioorg. Med. Chem.*, 2016, **24**, 4228–4240.
31 S. Holota, A. Kryshchyshyn, H. Derkach, Y. Trufin, I. Demchuk, A. Gzella, P. Grellier and R. Lesyk, *Bioorg. Chem.*, 2019, **86**, 126–136.
32 M. J. Nanjan, M. Mohammed, B. R. P. Kumar and M. J. N. Chandrasekar, *Bioorg. Chem.*, 2018, **77**, 548–567.
33 A. K. Ghosh, M. Brindisi, P. R. Nyalapatla, J. Takayama, J. R. Ella-Menye, S. Yashchuk, J. Agniswamy, Y. F. Wang, M. Aoki, M. Amano, I. T. Weber and H. Mitsuya, *Bioorg. Med. Chem.*, 2017, **25**, 5114–5127.
34 S. T. Tuncel, S. E. Gunal, M. Ekizoglu, N. Gokhan Kelekci, S. S. Erdem, E. Bulak, W. Frey and I. Dogan, *J. Mol. Struct.*, 2019, **1179**, 40–56.
35 M. F. Ansari, D. Idrees, M. I. Hassan, K. Ahmad, F. Avecilla and A. Azam, *Eur. J. Med. Chem.*, 2018, **144**, 544–556.
36 M. D. Rodrigues, P. B. G. S. Santiago, K. M. R. Marques, V. R. A. Pereira, M. C. A. B. Castro, J. C. L. L. Cantalice, T. G. Silva, M. L. Adam, S. C. Nascimento, J. F. C. Albuquerque and G. C. G. Militao, *Pharmacol. Rep.*, 2018, **70**, 446–454.
37 S. Yakaiah, P. S. V. Kumar, P. B. Rani, K. D. Prasad and P. Aparna, *Bioorg. Med. Chem. Lett.*, 2018, **28**, 630–636.
38 R. P. Singh, M. N. Aziz, D. Gout, W. Fayad, M. A. El-Manawaty and C. J. Lovely, *Bioorg. Med. Chem.*, 2019, **27**, 115047.
39 K. A. Szychowski, M. L. Leja, D. V. Kaminskyy, U. E. Binduga, O. R. Pinyazhko, R. B. Lesyk and J. Gmiński, *Chem. – Biol. Interact.*, 2017, **262**, 46–56.
40 N. Erlitzki, A. A. Farahat, A. Kumar, D. W. Boykin and G. M. K. Poon, *Biophys. Chem.*, 2019, **245**, 6–16.
41 E. A. Lafayette, S. M. V. Almeida, R. V. C. Santos, J. F. Oliveira, C. A. C. Amorim, R. M. F. Silva, M. G. R. Pitta, I. R. Pitta, R. O. Moura, L. B. C. Júnior, M. J. B. M. Rêgo and M. C. A. Lima, *Eur. J. Med. Chem.*, 2017, **136**, 511–522.
42 K. Kerboua and O. Hamdaoui, *Curr. Opin. Green Sustain. Chem.*, 2019, **18**, 84–89.
43 R. J. Wood, J. Lee and M. J. Bussemaker, *Ultrason. Sonochem.*, 2017, **38**, 351–370.
44 M. Lupacchini, A. Mascitti, G. Giachi, L. Tonucci, N. D'Alessandro, J. Martinez and E. Colacino, *Tetrahedron*, 2017, **73**, 609–653.
45 H. Hammoud, K. Elhabazi, R. Quillet, I. Bertin, V. Utard, E. Laboureyras, J. J. Bourguignon, F. Bihel, G. Simonnet, F. Simonin and M. Schmitt, *ACS Chem. Neurosci.*, 2018, **9**, 2599–2609.
46 P. Makam, P. K. Thakur and T. Kannan, *Eur. J. Pharm. Sci.*, 2014, **52**, 138–145.
47 N. O. Mahmoodi, B. Khalili, O. Rezaeianzade and A. Ghavidast, *Res. Chem. Intermed.*, 2016, **42**, 6531–6542.
48 T. Mosmann, *J. Immunol. Methods*, 1983, **65**, 55–63.
49 M. M. Silva, F. C. Savariz, E. F. Silva-Júnior, T. M. Aquino, M. H. Sarragiotto, J. C. C. Santos and I. M. Figueiredo, *J. Braz. Chem. Soc.*, 2016, **27**, 1558–1568.
50 C. M. Silva, M. M. Silva, F. S. Reis, A. L. T. G. Ruiz, J. E. Carvalho, J. C. C. Santos, I. M. Figueiredo, R. B. Alves, L. V. Modolo and A. Fátima, *J. Photochem. Photobiol., B*, 2017, **172**, 129–138.
51 K. M. R. Marques, M. R. Desterro, S. M. Arruda, L. N. A. Neto, M. C. A. Lima, S. M. V. Almeida, E. C. D. Silva, T. M. Aquino, E. F. Silva-Júnior, J. X. Araújo-Júnior, M. M. Silva, M. D. A. Dantas, J. C. C. Santos, I. M. Figueiredo, M. A. Bazin, P. Marchand, T. G. Silva and F. J. B. Mendonça Junior, *Curr. Top. Med. Chem.*, 2019, **19**, 1075–1091.
52 T. C. Braga, T. F. Silva, T. M. S. Maciel, E. C. D. Silva, E. F. Silva-Júnior, L. V. Modolo, I. M. Figueiredo,

J. C. C. Santos, T. M. Aquino and A. Fátima, *New J. Chem.*, 2019, **43**, 15187–15200.
53 M. D'Ascenzio, B. Bizzarri, C. De Monte, S. Carradori, A. Bolasco, D. Secci, D. Rivanera, N. Faulhaber, C. Bordón and L. Jones-Brando, *Eur. J. Med. Chem.*, 2014, **86**, 17–30.
54 A. Beauchard, A. Jaunet, L. Murillo, B. Baldeyrou, A. Lansiaux, J. Chérouvrier, L. Domon, L. Picot, C. Bailly, T. Besson and V. Thiéry, *Eur. J. Med. Chem.*, 2009, **44**, 3858–3865.
55 S. F. P. Braga, N. C. Fonseca, J. P. Ramos, E. M. Souza-Fagundes and R. B. Oliveira, *Braz. J. Pharm. Sci.*, 2016, **52**, 299–307.
56 M. M. Silva, E. O. O. Nascimento, E. F. Silva-Júnior, J. X. Araújo-Júnior, C. C. Santana, L. A. M. Grillo, R. S. Oliveira, P. R. R. Costa, C. D. Buarque, J. C. C. Santos and I. M. Figueiredo, *Int. J. Biol. Macromol.*, 2017, **96**, 223–233.
57 R. A. Marques, A. O. C. V. Gomes, M. V. Brito, A. L. P. Santos, G. S. Silva, L. B. Lima, F. M. Nunes, M. C. Mattos, F. C. E. Oliveira, C. Ó. Pessoa, M. O. Moraes, A. Fátima, L. L. Franco, M. M. Silva, M. D. A. Dantas, J. C. C. Santos, I. M. Figueiredo, E. F. Silva-Júnior, T. M. Aquino, J. X. Araújo-Júnior, M. C. F. Oliveira and A. A. Leslie Gunatilaka, *J. Photochem. Photobiol., B*, 2018, **179**, 156–166.
58 S. Das, C. J. Silva, M. M. Silva, M. D. A. Dantas, A. Fátima, A.L.T. Góis Ruiz, C. M. Silva, J. E. Carvalho, J. C. C. Santos, I. M. Figueiredo, E. F. Silva-Júnior, T. M. Aquino, J. X. Araújo-Júnior, G. Brahmachari and L. V. Modolo, *J. Adv. Res.*, 2018, **9**, 51–61.
59 C. B. P. Kumar, M. S. Raghu, K. N. N. Prasad, S. Chandrasekhar, B. K. Jayanna, F. A. Alharthi, M. K. Prashanth and K. Y. Kumar, *New J. Chem.*, 2021, **45**, 403–414.
60 F. C. Savariz, M. A. Foglio, A. L. T. Goes Ruiz, W. F. Costa, M. Magalhães Silva, J. C. C. Santos, I. M. Figueiredo, E. Meyer, J. E. Carvalho and M. H. Sarragiotto, *Bioorg. Med. Chem.*, 2014, **22**, 6867–6875.
61 M. A. Loza-Mejía, K. Maldonado-Hernández, F. Rodríguez-Hernández, R. Rodríguez-Sotres, I. González-Sánchez, A. Quintero, J. D. Solano and A. Lira-Rocha, *Bioorg. Med. Chem.*, 2008, **16**, 1142–1149.
62 A. M. Macan, N. Perin, S. Jakopec, M. Mioč, M. R. Stojković, M. Kralj, M. Hranjec and S. Raić-Malić, *Eur. J. Med. Chem.*, 2020, **185**, 111845.
63 M. R. Aouad, M. A. Almehmadi, N. Rezki, F. F. Al-blewi, M. Messali and I. Ali, *J. Mol. Struct.*, 2019, **1188**, 153–164.
64 A. A. Phadte, S. Banerjee, N. A. Mate and A. Banerjee, *Biochem. Biophys. Rep.*, 2019, **18**, 100629.
65 A. K. Williams, S. C. Dasilva, A. Bhatta, B. Rawal, M. Liu and E. A. Korobkova, *Anal. Biochem.*, 2012, **422**, 66–73.
66 M. Sirajuddin, S. Ali and A. Badshah, Drug–DNA interactions and their study by UV–Visible, *J. Photochem. Photobiol., B*, 2013, **124**, 1–19.
67 Z. Chi, R. Liu, Y. Sun, M. Wang, P. Zhang and C. Gao, *J. Hazard. Mater.*, 2010, **175**, 274–278.
68 M. M. Silva, T. S. Macedo, H. M. P. Teixeira, D. R. M. Moreira, M. B. P. Soares, A. L. C. Pereira, V. L. Serafim, F. J. B. Mendonça-Júnior, M. C. A. Lima, R. O. Moura, E. F. Silva-Júnior, J. X. Araújo-Júnior, M. D. A. Dantas, E. O. O. Nascimento, T. M. S. Maciel, T. M. Aquino, I. M. Figueiredo and J. C. C. Santos, *J. Photochem. Photobiol., B*, 2018, **189**, 165–175.
69 S. Patai, *The Chemistry of the Hydrazo*, Azo and Azoxy Groups, 2rd edn, Wiley & Sons, Mew York, 1997.
70 F. C. Abreu, F. S. Paula, D. C. M. Ferreira, V. B. Nascimento, J. C. D. Lopes, A. M. C. Santos, M. M. Santoro, C. E. Salas and M. O. F. Goulart, *Sensors*, 2008, **8**, 1519–1538.
71 S. Murugavel, C. S. J. P. Stephen, R. Subashini and D. AnanthaKrishnan, *J. Photochem. Photobiol., B*, 2017, **173**, 216–230.